V International Conference on Simulation for Additive Manufacturing
Sim-AM 2025
F. Auricchio, M. Carraturo and S. Morganti (Eds)

ENERGY-BASED FORM-FINDING OF COLUMN-LIKE LATTICE ELEMENTS

M. BRUGGI, C. GUERINI AND G. NOVATI

Department of Civil and Environmental Engineering
Politecnico di Milano
Piazza Leonardo da Vinci 32, 20133, Milano, Italy
e-mail: matteo.bruggi@polimi.it carlo.guerini@polimi.it giorgio.novati@polimi.it

Key words: numerical simulations, Additive Manufacturing (AM), computational modeling

Abstract. Wire-and-Arc Additive Manufacturing (WAAM) enables the construction of lattice structures composed of branches with constant cross-sectional area, offering flexibility in shaping the overall geometry. This work explores the design of spatial networks tailored for WAAM, focusing on column-like meso-elements through a hybrid strategy that combines optimization techniques with funicular analysis. Structural equilibrium is modeled using the force density method, which expresses the problem in terms of the force-to-length ratio for each branch. Sector symmetry imposed on the column-like elements leads to the arising of independent branch sets. The optimization framework focuses on subsets of force densities to identify configurations that minimize strain energy. To ensure structural integrity and geometric control, additional constraints are imposed on node positioning, branch length variability, and the radius of the latticed cross-section. The optimization is performed via sequential convex programming, applied across various grid typologies. The resulting designs are validated through linear finite element analysis, including linear buckling assessment. Key features of the optimized layouts, along with the characteristics and limitations of the underlying methodology, are examined and discussed.

1 INTRODUCTION

Promising applications of metal 3D printing in construction are increasingly centered around Wire-and-Arc Additive Manufacturing (WAAM) [1]. This technique enables the fabrication of optimized structural layouts by leveraging automated production and minimizing material usage. WAAM is particularly suitable for constructing lattice structures across multiple scales, including meso-elements such as the lattice column investigated in this study [2]. The adopted "dot-by-dot" deposition strategy allows for the creation of networks composed of slender bars with fixed cross-sections, as primarily dictated by the printing equipment and process parameters.

Lattice shells typically exhibit double curvature and consist of branches that predominantly carry axial forces [3]. Their optimal geometries can be effectively explored using equilibrium-based methods, such as funicular analysis [4, 5]. These reticulated shells are modeled as networks of struts and ties with defined connectivity. Supports are assigned to restrained nodes, while unrestrained nodes are governed by equilibrium conditions under applied point loads. Although the equilibrium equations for unrestrained nodes are nonlinear in terms of nodal coordinates, they become linear and decoupled across spatial directions when reformulated using force densities defined as the force-to-length ratio

in each branch, see the Force Density Method (FDM)[6]. This reformulation facilitates form-finding, especially when integrated with optimization strategies [7, 8, 9].

In this work, complementary strain energy is selected as the objective function. As demonstrated in [10], minimizing complementary energy promotes compatibility among equilibrated configurations iteratively generated via the Force Density Method (FDM), thereby dealing with minimum compliance design without solving the full elastic equilibrium equations. A specialized version of the approach in [10] is developed here, embedding FDM within a multi-constrained optimization framework that exploits rotational symmetry. The resulting problem is efficiently solved using sequential convex programming techniques [11], originally designed for large-scale, multi-constrained size optimization in elastic structures [12]. The optimization handles a reduced set of independent force densities derived from the imposed rotational symmetry. The objective function, i.e. complementary energy, coincides with strain energy and is twice the structural compliance under the adopted linear elastic framework. Geometric constraints are introduced to regulate member lengths (to accommodate manufacturing limitations and prevent local buckling), the minimum radius of the column-like meso-element (to prevent global buckling), and the vertical position of the top nodes (to prescribe the element's height).

Subsequent sections provide an overview of the Force Density Method as applied to rotationally symmetric structures [13] and present the multi-constrained optimization problem. Numerical studies assess the proposed methodology and explore lattice column configurations with varying connectivity. The results are validated through linear finite element analyses, including linear buckling analyses, using mechanical parameters from the experimental study in [14]. Finally, conclusions are drawn regarding the effectiveness of the proposed simplified procedure and the quality of the resulting designs.

2 FORM-FINDING

The Force Density Method (FDM) [6] is employed as the "state equation" within the optimization framework to ensure equilibrium in spatial lattice structures. A funicular network is composed of $n_s = n + n_f$ nodes and m branches, each capable of carrying axial forces only. The Cartesian coordinate system, with origin at point O, is defined by the axes x, y, and z. Following the notation in [6], the vectors $\mathbf{x}_s$, $\mathbf{y}_s$, and $\mathbf{z}_s$ collect the coordinates of all n_s nodes. These are partitioned into $\mathbf{x}$, $\mathbf{y}$, $\mathbf{z}$ for the n unrestrained nodes, where external loads are applied, and $\mathbf{x}_f$, $\mathbf{y}_f$, $\mathbf{z}_f$ for the n_f restrained nodes, where reactions occur. The connectivity of the lattice is described by the matrix $\mathbf{C}_s$, with sub-matrices $\mathbf{C}$ and $\mathbf{C}_f$ corresponding to unrestrained and restrained nodes, respectively. In particular, $\mathbf{C}_h$ is the subset of $\mathbf{C}_s$ which corresponds to the unrestrained nodes in the h direction, whereas $\mathbf{C}_{fh}$ refers to the restrained ones along the same axis. The coordinate differences along each axis are represented by the vectors:

$$\begin{aligned} \mathbf{u} &= \mathbf{C}_s \mathbf{x}_s, \\ \mathbf{v} &= \mathbf{C}_s \mathbf{y}_s, \\ \mathbf{w} &= \mathbf{C}_s \mathbf{z}_s. \end{aligned} \tag{1}$$

Force densities, defined as the ratio of axial force to member length, are stored in the vector $\mathbf{q} = \mathbf{L}^{-1}\mathbf{s}$, where $\mathbf{s}$ contains the axial forces in the m branches, and $\mathbf{L} = \mathrm{diag}(\mathbf{l})$ is the diagonal matrix of branch lengths $l_i = \sqrt{u_i^2 + v_i^2 + w_i^2}$. Only vertical loads are considered in this study, represented by the vector $\mathbf{p}_z$. With the introduction of $\mathbf{q}$, the equilibrium conditions for the unrestrained nodes reduce to

a system of linear equations, decoupled across the three spatial directions:

$$\begin{aligned}
&\mathbf{C}_x^T\mathbf{Q}\mathbf{C}_x\mathbf{x}+\mathbf{C}_x^T\mathbf{Q}\mathbf{C}_{fx}\mathbf{x}_f=\mathbf{0},\\
&\mathbf{C}_y^T\mathbf{Q}\mathbf{C}_y\mathbf{y}+\mathbf{C}_y^T\mathbf{Q}\mathbf{C}_{fy}\mathbf{y}_f=\mathbf{0},\\
&\mathbf{C}_z^T\mathbf{Q}\mathbf{C}_z\mathbf{z}+\mathbf{C}_z^T\mathbf{Q}\mathbf{C}_{fz}\mathbf{z}_f=\mathbf{p}_z,
\end{aligned} \tag{2}$$

where $\mathbf{Q}=\text{diag}(\mathbf{q})$.

In this study, the focus is on column-like meso-elements exhibiting rotational symmetry. This symmetry allows the form-finding process to be governed by a reduced set of independent force densities, denoted by $\bar{\mathbf{q}}$, see [13]. The full set of force densities is then expressed as:

$$\mathbf{q}=\mathbf{B}\bar{\mathbf{q}}, \tag{3}$$

where the matrix B_{jk} encodes the symmetry relations: $B_{jk}=1$ if $q_j=\bar{q_k}$, and $B_{jk}=0$ otherwise.

3 MULTI-CONSTRAINED OPTIMIZATION

A multi-constrained problem of optimal design is formulated in terms of any sub-set of independent force densities $\bar{\mathbf{q}}$, with the aim of designing lightweight lattices for minimum compliance.

One has:

$$\begin{cases}
\min\limits_{\bar{q_k}} \; f & \text{(4a)}\\
\quad \text{s.t.} \quad \mathbf{C}_x^T\mathbf{Q}\mathbf{C}_x\mathbf{x}+\mathbf{C}_x^T\mathbf{Q}\mathbf{C}_{fx}\mathbf{x}_f=\mathbf{0}, & \\
\qquad \mathbf{C}_y^T\mathbf{Q}\mathbf{C}_y\mathbf{y}+\mathbf{C}_y^T\mathbf{Q}\mathbf{C}_{fy}\mathbf{y}_f=\mathbf{0}, & \text{(4b)}\\
\qquad \mathbf{C}_z^T\mathbf{Q}\mathbf{C}_z\mathbf{z}+\mathbf{C}_z^T\mathbf{Q}\mathbf{C}_{fz}\mathbf{z}_f=\mathbf{p}_z, & \\
\qquad \mathbf{q}=\mathbf{B}\bar{\mathbf{q}}, & \text{(4c)}\\
\qquad \left(\dfrac{l_j}{l_{min}}\right)^2 \geq 1 \quad \text{for } \; j=1...m, & \text{(4d)}\\
\qquad \left(\dfrac{l_j}{l_{max}}\right)^2 \leq 1 \quad \text{for } \; j=1...m, & \text{(4e)}\\
\qquad \dfrac{x_i^2+y_i^2}{r_{min}^2} \geq 1 \quad \text{for } \; i=1...n, & \text{(4f)}\\
\qquad z_{h_t} \geq z_t^{min} \quad \text{for } \; h=1...n_t, & \text{(4g)}
\end{cases}$$

In the above discrete problem, the objective function is computed as:

$$f=\frac{1}{2}\sum\nolimits_{j=1}^{m}\left(\frac{s_j}{A}\frac{s_j}{EA}Al_j\right)=\frac{1}{2EA}\mathbf{s}^T\mathbf{L}\mathbf{s}=\frac{1}{2EA}\mathbf{q}^T\mathbf{L}^3\mathbf{q}, \tag{5}$$

where A denotes the cross-sectional area and E the elastic modulus of the material, both considered uniform across all branches owing to the consistency of the "dot-by-dot" WAAM process (aside from printing uncertainties), see e.g. [14].

For statically indeterminate structures, the set of force densities $\mathbf{q}$ associated with a given geometry is non-unique. Nevertheless, as discussed and tested in [10], Eqn. (4) is expected to tend at convergence to the force density distribution that corresponds to the solution of the linear elastic equilibrium.

This stems from the fact that, among all admissible stress states satisfying equilibrium, the one that also fulfills compatibility conditions minimizes the complementary strain energy.

The system of Eqn. (4b) expresses the equilibrium conditions for the unrestrained nodes along the three spatial directions. This enables the computation of the nodal coordinates $\mathbf{x}$, $\mathbf{y}$, $\mathbf{z}$, based on the complete set of force densities contained in $\mathbf{q}$. The connection between $\mathbf{q}$ and the minimization variables $\bar{\mathbf{q}}$ is established through Eqn. (4c).

Eqns. (4d) and (4e) are set of local constraints that are employed to prescribe the minimum (l_{min}) and maximum (l_{max}) value of the length of each branch in the optimal network. The coordinate difference of the connected points given in Eqn. (1) are used to enforce these geometric constraints in a straightforward way. They also play a key role in regularizing the optimization problem. Imposing a lower bound l_{min} helps avoid overly dense regions that could pose challenges during printing, while setting an upper bound l_{max} enforces a limit on member slenderness, thereby reducing the risk of branch buckling.

Eqn. (4f) is used to enforce a minimum radius (r_{min}) for the cross-section of the column-like meso-element, with the aim of maintaining a minimum second moment of area to prevent column buckling.

The inequalities in Eqn. (4g) enforce a minimum elevation for a subset of the nodal coordinates $\mathbf{z}$, i.e. those of the top nodes. Indeed, z_t^{min} is the minimum height of the column.

The arising multi-constrained minimization problem is solved by means of the Method of Moving Asymptotes [11], see the discussion in Section 1. Being MMA a first order approach, the sensitivity of the objective function and constraints with respect to the force densities $\mathbf{q}$ is needed, see e.g. [8] and [10]. The chain rule may be used to compute the derivatives with respect to the minimization variables $\bar{\mathbf{q}}$, see Eqn. (4c). It is remarked that Eqns. (4b) are solved for the current set of $\bar{\mathbf{q}}$ (and $\mathbf{q}$). Also, due to the limited number of minimization unknowns, the enforcement of the local constraints in Eqns. (4d)–(4g) does not call for the implementation of ad hoc techniques to preserve numerical efficiency, see in particular [15].

4 NUMERICAL STUDIES

A lattice column is addressed, inspired by the investigations presented in [2, 16] in the field of Wire-and-Arc Additive Manufacturing (WAAM), see also [1, 17]. Using the "dot-by-dot" deposition technique with a 304L stainless steel wire, bars with a nominal diameter of $6\,$mm can be fabricated [8]. A column-like meso-element with bottom and top fixed radius equal to $r = 0.35\,$m is herein investigated, considering three types of lattice, whose connectivity is represented in Figure 1. The lattice type A is diamond-like, whereas type B and type C are diagrid-like lattices.

The vertical load is applied at the $16/24$ top nodes, with a resultant of $10\,$kN. These top nodes are restrained along the x and y axes, whereas the $16/24$ bottom nodes are restrained in the three Cartesian direction. The order of rotational symmetry enforced by Eqn. (4c) is 16 for lattice types A and B, and 12 for lattice type C.

The minimization of the structural compliance for the applied loads is addressed by implementing the formulation in Eqn. (4), with the following parameters: $l_{min} = 0.06\,$m, $l_{max} = 0.12\,$m, $r_{min} = 0.075\,$m, and $z_t^{min} = 2.5\,$m. Following [8] and [14], it is assumed that $E = 100\,$GPa. According to the referenced investigations, a single bar can withstand: i) $7\,$kN in tension, and ii) $3\,$kN in compression for a slenderness equal to 80, which corresponds to the herein enforced $l_{max} = 0.12\,$m.

If not differently specified, the optimization is initialized by using a homogeneous distribution of compressive force densities. For all optimized lattice configurations, the constraints defined in Equation (4g) are active, ensuring that the height of the column-like meso-element is consistently

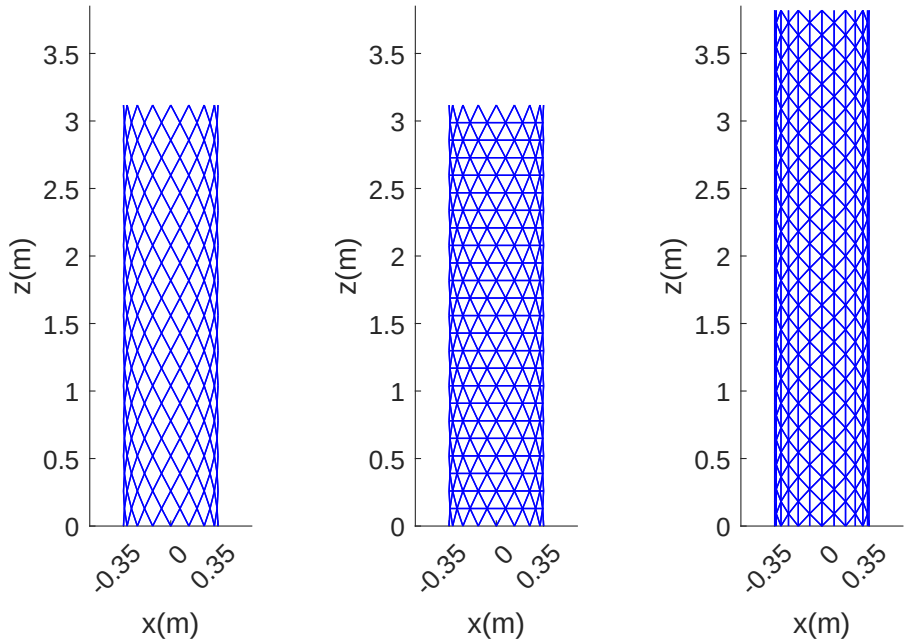

Figure 1: Connectivity of the members for a column-like meso-element: lattice type A (left), lattice type B (center), lattice type C (right).

equal to z_t^{min}. Similarly, subsets of the constraints from both Equations (4e)–(4f) are also active, indicating that each optimal layout includes branches whose lengths attain the prescribed bounds l_{min} and l_{max}. Finally, it is reported that all computed solutions satisfy the full set of imposed constraints, i.e. they are feasible solutions to the stated minimization problem.

For each of the achieved optimal designs, a finite element model has been created using the software [18], where each branch has been discretized into five beam elements. Bending-resistant connections were employed to simulate the continuous deposition process, while bending-resistant members were implemented to approximate the buckling load, including effects from branch buckling. Linear elastic finite element analyses have been performed to check that the distribution obtained at convergence through the proposed form-finding approach for reticulated shells is a good approximation of the solution of the linear elastic equilibrium. Additionally, analyses have been performed to compute the critical load multiplier, i.e. the first eigenvalue of the associated linear buckling problem.

The optimal layout found for the lattice type A is represented in Figure 2, along with a map of the forces $\mathbf{s} = \mathbf{L}\mathbf{q}$ computed at convergence. The set $\mathbf{s}$ is in equilibrium with the prescribed vertical load, as per Eqns. (4b). The total length equals $87.8\,\mathrm{m}$. Overall, the diamond-like patterns is preserved at the extreme, whereas in the central part of the column the bearing structure tends to align to the vertical direction. The minimum radius of the column is equal to r_{min}. The force distribution obtained at convergence through the proposed form-finding approach matches the solution of the linear elastic equilibrium, see Figure 3. The critical load multiplier is 2.76.

The optimal result for the lattice type B and the relevant map of forces are given in Figure 4. In this case an initialization with tensile force densities has been adopted for the elements in the hoops. At the ends of the column the form-finding retrieves a diagrid-like pattern that is not far from the diamond-like layout of Figure 2. The overall length is $116.8\,\mathrm{m}$, whereas the minimum radius of the column is larger than r_{min}. Again, a very good match is reported comparing the force distribution in

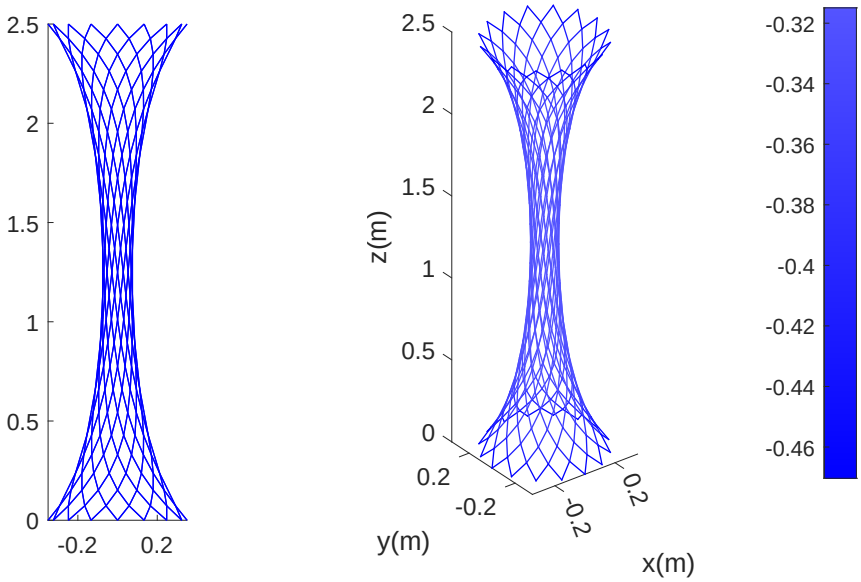

Figure 2: Optimal design (left) and map of the element forces (right, in kN) for lattice type A.

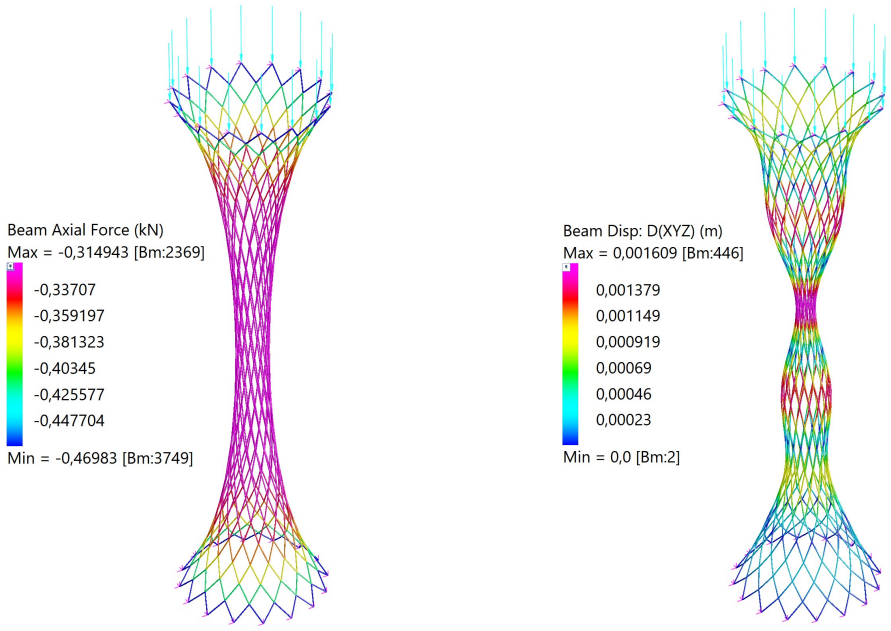

Figure 3: Element forces (left) and first buckling mode (right, $\lambda = 2.76$) from FEA of the optimal design for lattice type A.

Figure 4(right) to the solution of the linear elastic equilibrium, see Figure 5(left). The critical load multiplier corresponding to the design found for the diagrid-like pattern B reads 11.21, a much larger value than that read for the diamond-like lattice type A.

In Figure 6, convergence curves reported for the optimization of the lattice type B are given. They refer to the history plot of the objective function (scaled to its initial value) and of the feasibility of the

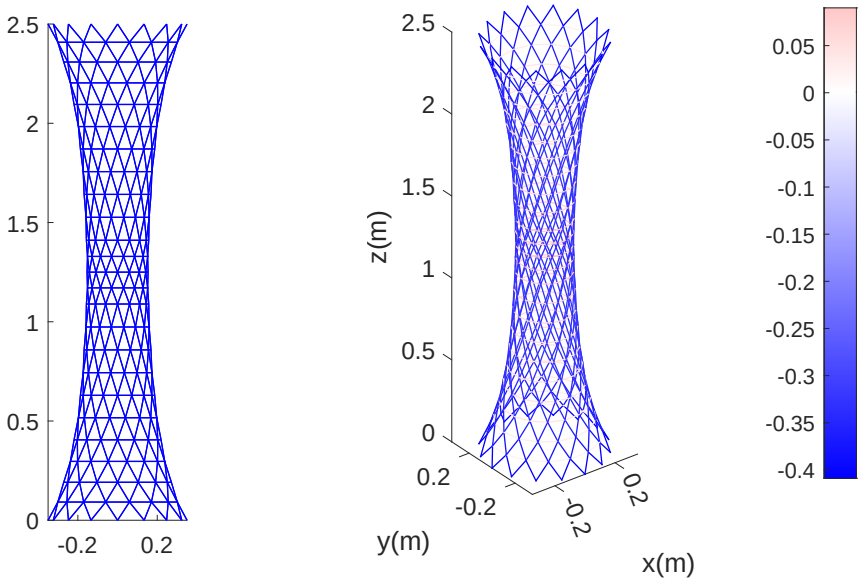

Figure 4: Optimal design (left) and map of the element forces (right, in kN) for lattice type B.

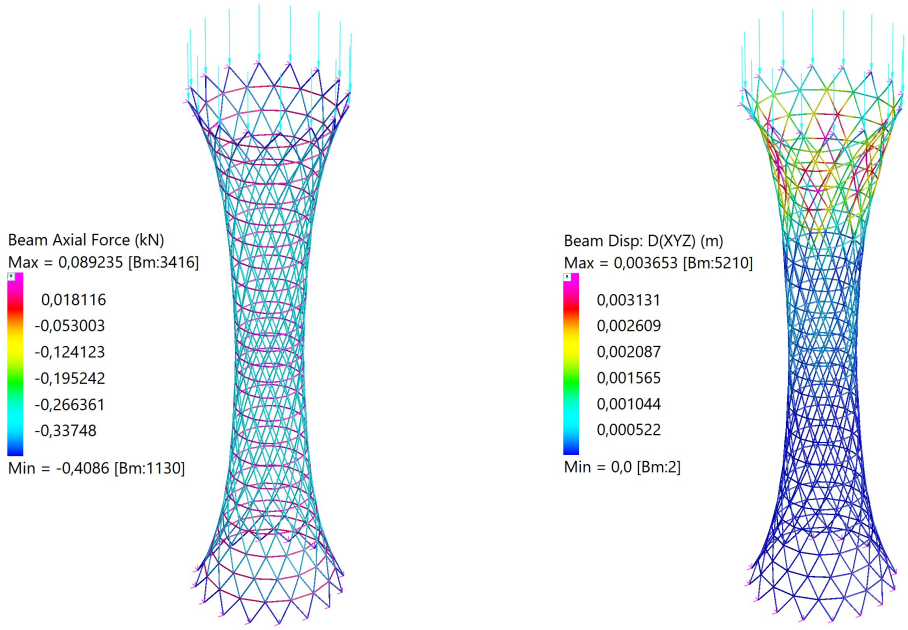

Figure 5: Element forces (left) and first buckling mode (right, $\lambda = 11.21$) from FEA of the optimal design for lattice type B.

constraints (equal to one when all the enforcements are fulfilled). A few iterations are needed to reach a feasible region of the design domain, whereas smooth convergence is reported in the subsequent steps.

An additional simulation was carried out for lattice type B, enforcing a minimum radius of $r_{min} = 3 \cdot 0.075\,\mathrm{m}$. Figure 7 presents a map of the forces acting on the optimized column, along with the

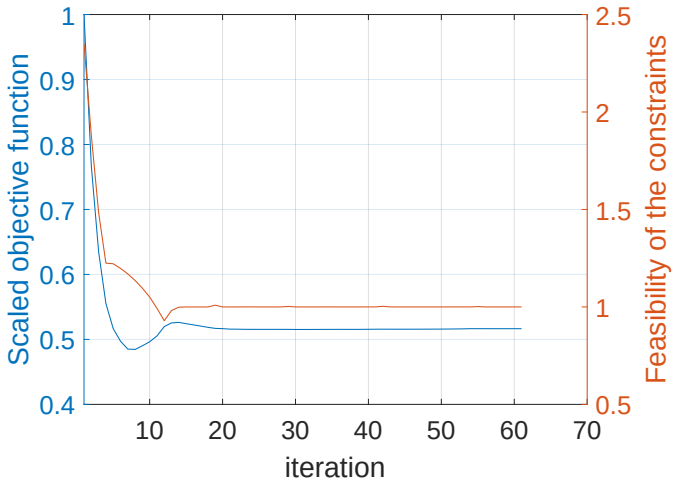

Figure 6: Convergence plots for the form-finding using lattice type B.

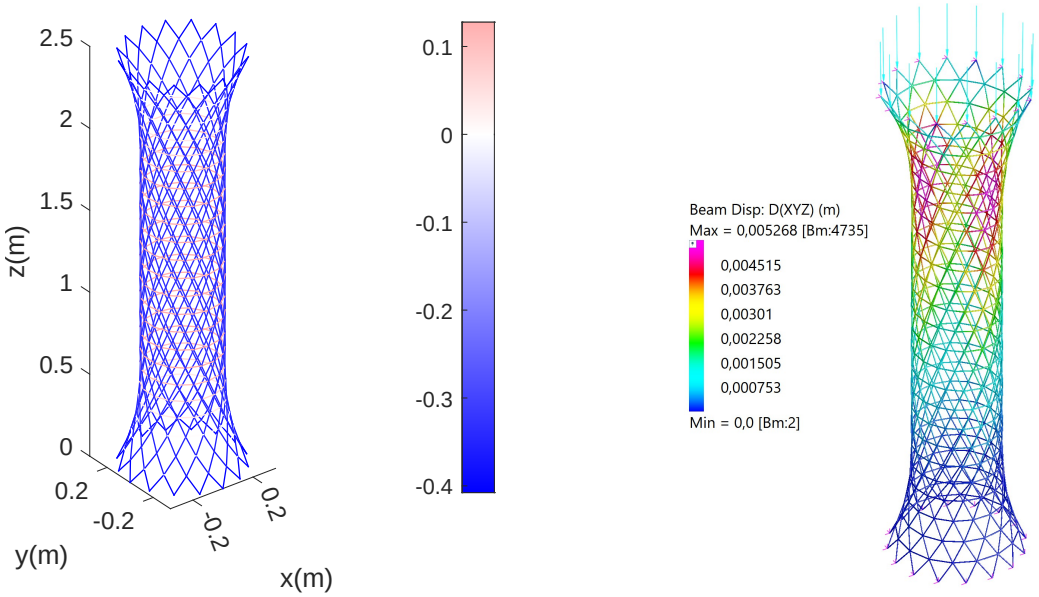

Figure 7: Map of the element forces (left, in kN) and first buckling mode (right, $\lambda = 6.72$) from FEA for a variation of the optimal design with lattice type B.

first buckling mode obtained via finite element analysis (FEA). This mode emerges at a critical load multiplier of $\lambda = 6.72$, which is lower than the value found for the design with a smaller lattice cross-section, see Figures 4 and 5. This result highlights that controlling the minimum radius of the cross-section is a straightforward method to ensure a minimum flexural stiffness. While this approach is beneficial for mitigating column buckling, it cannot substitute for a comprehensive stability-oriented design strategy, as that presented in [10], which must account for global and lattice buckling phenomena.

The result obtained when using lattice type C and the relevant map of forces are depicted in Figure 8. The overall length is 151.6 m. As for the lattice type B, the minimum radius of the column is larger than r_{min}. The optimal design is characterized by a central region made of bars that are nearly vertical

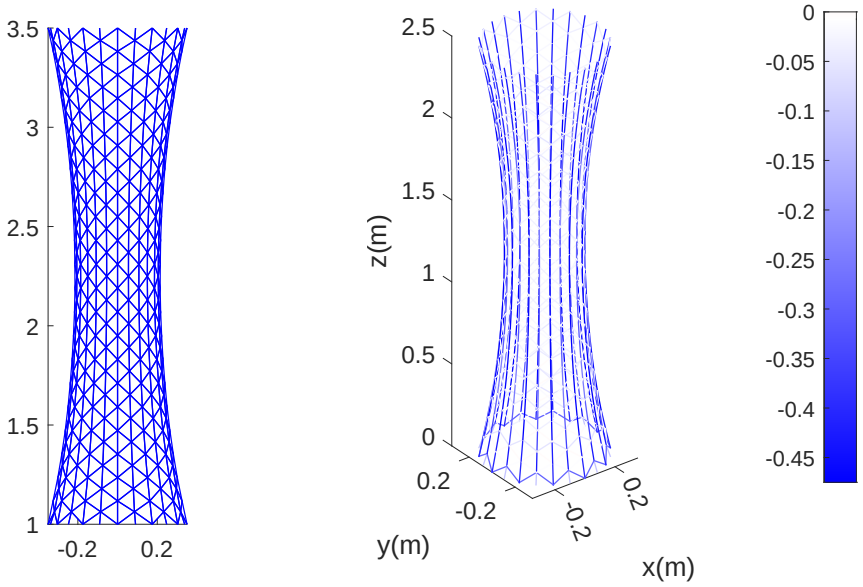

Figure 8: Optimal design (left) and map of the element forces (right, in kN) for lattice type C.

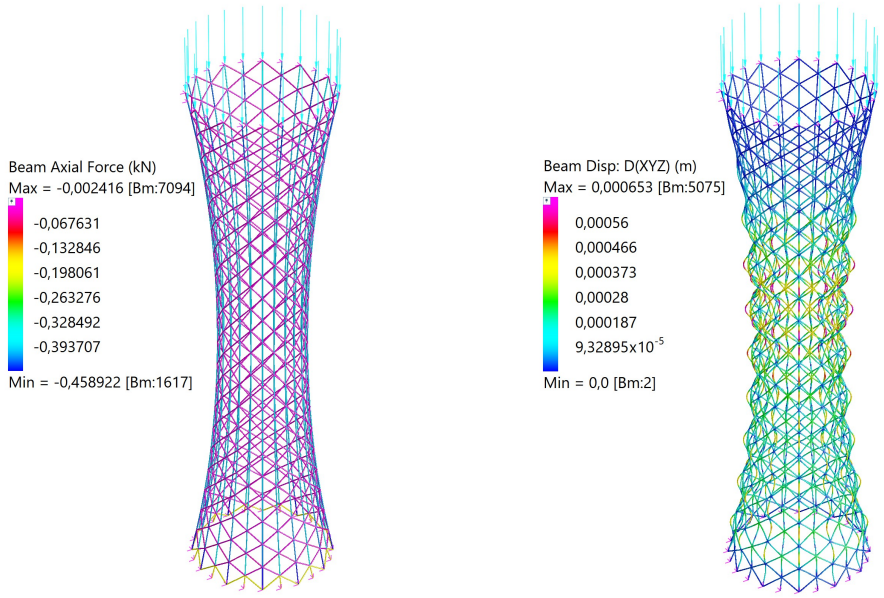

Figure 9: Element forces (left) and first buckling mode (right, $\lambda = 19.91$) from FEA of the optimal design for lattice type C.

and transfer most of the vertical forces to the ground restraints. The diagrid scheme is entirely active only at the lower end of the column. Again, the force distribution found at convergence through the proposed form-finding approach is in agreement with the solution of the linear elastic equilibrium, see Figure 9. Among the three results, the optimal design for lattice type C exhibits the highest critical load multiplier (19.91), indicating better stability under compressive forces.

It is finally remarked that neither stress constraints nor overhang constraints have been imple-

mented in this numerical investigation, see [8]. Indeed, the achieved force maps were found to be compatible with the estimated capacity of the bars. Concerning overhang, while optimal results for lattices type A and type C are marginally affected by this issue, the printing strategies discussed in [1] and [16] can be referred to when tackling the hoops of the optimal solution of lattice type B.

5 CONCLUDING REMARKS

In this contribution, a numerical tool has been implemented to address the design of column-like meso-elements through funicular analysis. As investigated in recent literature, the force density method can be conveniently applied to model the equilibrium of spatial networks of bars, especially when coupling the form-finding tool with optimization routines. Exploiting sector symmetry on column-like elements leads to the emergence of independent branch sets, simplifying the design process.

An optimization framework based on sequential convex programming has been used to minimize strain energy by selectively tuning subsets of force densities, while satisfying geometric and structural constraints such as node positioning, branch length variability, and the minimum radius of the latticed cross-section. Numerical tests have been performed on a diamond-like lattice and two types of diagrid-like patterns, adopting mechanical parameters from available experimental studies.

The resulting configurations have been validated through linear finite element analysis, including buckling assessment. The outcomes confirm the applicability of the proposed approach in generating structurally efficient layouts that comply with the constraints imposed by WAAM technology, while requiring limited computational cost. For a more robust control of the instabilities affecting structural elements composed of reticulated shells, one should consider the adoption of an eigenvalue-constrained procedure, such as the one proposed in [10], or the use of more advanced design and analysis methods accounting for nonlinear geometry

Acknowledgements

Funded by the European Union - Next Generation EU, Mission 4, Component 1
CUP D53D23003900006, PRIN 2022P7FLNC “LATTICE” (Lattice meso-elements for a new class of green steel structures).

REFERENCES

[1] Costello, S. C. A., Cunningham, C. R., Xu, F., Shokrani, A., Dhokia, V., and Newman, S.T. 2023. “The state-of-the-art of wire arc directed energy deposition (WA-DED) as an additive manufacturing process for large metallic component manufacture.” Int J Comput Integr Manuf, 36, no. 3, 469-510.

[2] Laghi, V., Palermo, M., Gasparini, G., and Trombetti, T. 2020. “Computational design and manufacturing of a half-scaled 3D-printed stainless steel diagrid column.” Addit Manuf, 36, 101505.

[3] Rozvany, G. I. N. and Prager, W. 1979. “A new class of structural optimization problems: Optimal archgrids.” Comput Methods Appl Mech Eng, 19, no. 1, 127-150.

[4] O’Dwyer, D. 1999. “Funicular analysis of masonry vaults.” Comput Struct, 73, no. 1-5, 187–197.

[5] Adriaenssens, S., Block, P., Veenendaal, D. and Williams, C. 2014. Shell structures for architecture: Form finding and optimization, Routledge.

[6] Schek, H.-J. 1974. "The force density method for form finding and computation of general networks." Comput Methods Appl Mech Eng, 3, no. 1, 115–134.

[7] Bruggi, M. 2020. "A constrained force density method for the funicular analysis and design of arches, domes and vaults." Int J Solids Struct, 193–194, 251–269.

[8] Bruggi, M., Laghi, V. and Trombetti T. 2023. "Stress-based form-finding of gridshells for Wire-and-Arc Additive Manufacturing considering overhang constraints." Eng Struct, 279, 115654.

[9] Liew, A. 2020. "Constrained Force Density Method optimisation for compression-only shell structures." Structures, 28, 1845–1856.

[10] Bruggi, M., Guerini, C. 2025. "Energy-based form-finding of reticulated shells accounting for eigenvalue buckling." Compos Struct, 354(118742), 118742.

[11] Svanberg, K. 1987. "The method of moving asymptotes—a new method for structural optimization," Int. J Numer Methods Eng, 24, 2, 359–373.

[12] Christensen, P. W. and Klarbring, A. 2008. An introduction to structural optimization, Springer.

[13] Bruggi, M., Guerini, C., Novati, G. 2024. "Optimal design of lattice structure for column-like Meso-elements." 16th World Congress on Computational Mechanics, Lisbon, Portugal.

[14] Laghi, V., Girelli, V. A., Gasparini, G., Trombetti, T., Palermo, M. 2024. "Investigation on the elastic flexural stiffness of dot-by-dot wire-and-arc additively manufactured stainless steel bars." Eng Struct, 306(117680).

[15] Bertsekas, D.P. 1999. Nonlinear programming, 2nd edn. Athena Scientific.

[16] Yu, Z., Pan, Z., Ding, D., Polden, J., He, F., Yuan, L. and Li, H. 2021. "A practical fabrication strategy for wire arc additive manufacturing of metallic parts with wire structures." Int J Adv Manuf Technol, 115, no. 9-10, 3197–3212.

[17] Huang, C., Kyvelou, P., and Gardner L. 2023. "Stress-strain curves for wire arc additively manufactured steels." Eng Struct, 279, 115628.

[18] "Strand7", Strand7 Pty Ltd, Release 3, 2021, www.strand7.com/r3